

# Performance of Ultrasound Vector Velocity Measurement at Great Depths

S. Rossi

Dept. of Information Engineering  
University of Florence  
50139 Florence, Italy  
stefano.rossi@unifi.it

A. Ramalli

Dept. of Cardiovascular Sciences  
KU Leuven  
3000 Leuven, Belgium  
alessandro.ramalli@kuleuven.be

S. Ricci

Dept. of Information Engineering  
University of Florence  
50139 Florence, Italy  
stefano.ricci@unifi.it

R. Matera

Dept. of Information Engineering  
University of Florence  
50139 Florence, Italy  
riccardo.matera@unifi.it

F. Guidi

Dept. of Information Engineering  
University of Florence  
50139 Florence, Italy  
francesco.guidi@unifi.it

E. Boni

Dept. of Information Engineering  
University of Florence  
50139 Florence, Italy  
enrico.boni@unifi.it

P. Tortoli

Dept. of Information Engineering  
University of Florence  
50139 Florence, Italy  
piro.tortoli@unifi.it

**Abstract**— Ultrasound assessment of blood velocity vectors is usually performed on vessels, like the carotid artery, placed at shallow depths, while only few studies have been presented so far on the investigation of deep vessels. Some vector methods present clear disadvantages at great depth: for example, in multi-beam vector Doppler the inter-beam angle dramatically reduces due to the limited aperture. This problem, in principle, does not affect speckle tracking methods, which could potentially operate even with small transmission apertures. The aim of this work is to investigate the behavior, at different depths, of high frame rate Vector Flow Imaging methods based on the transmission of plane waves. Simulations show that accuracies better than 10% can be obtained for depths shallower than 6 cm but, at higher depths, the performance is significantly affected by the azimuthal broadening of the pressure field.

**Keywords**—vector velocity imaging, plane waves, deep vessels, RF data acquisition, open platform, ULA-OP

## I. INTRODUCTION

Cardiovascular diseases are widely diffused, and strong efforts are spent by researchers to understand the pathological processes that origin, for instance, blood clots and atherosclerosis. Ultrasound (US) techniques play here an important role since they are used in the clinic to detect the presence of constrictions or occlusions of arteries. Recently, vector Doppler methods have been shown capable of producing detailed maps of blood flow [1]–[3]. However, while most of the studies were performed on vessels placed at shallow depths, like the carotid artery, the performance of vector methods in the examination of deep vessels is still underexplored, in spite of its importance e.g. for detection of aortic diseases [4]. Indeed, the accuracy of methods based on the multi-beam approach [1]–[3], [5]–[7] or on transverse oscillations [8], [9] is typically worse at deep depths due to the limited physical aperture of the array [10]. On the other hand, speckle-tracking methods, either based on a 2D cross correlation [11], [12] or on different velocity estimators

A. Ramalli was supported by the European Union’s Horizon 2020 research and innovation programme under the Marie Skłodowska-Curie grant agreement No 786027 (ACOUSTIC project).

[13]–[15], should not be affected by such problems. The goal of this paper was to test to what extent the performance of the high frame rate vector flow imaging (HFR-VFI) method described in [13]–[15], which is based on the transmission of plane waves and on frequency domain phase estimation, depends on the exploration depth. Simulations were conducted for a linear array investigating with different orientations a blood flow at depths in the range 2–10 cm.

## II. METHODS

### A. High frame rate vector flow imaging basics

The HFR-VFI method reconstructs 2D maps of velocity vectors by processing consecutive sets of radiofrequency (RF) echo signals received after the transmission of unsteered plane waves (PWs) through the region of interest. PWs are transmitted at pulse repetition frequency (PRF). For each transmitted PW, a parallel beamformer reconstructs an RF image so that the frame rate is equal to the PRF.

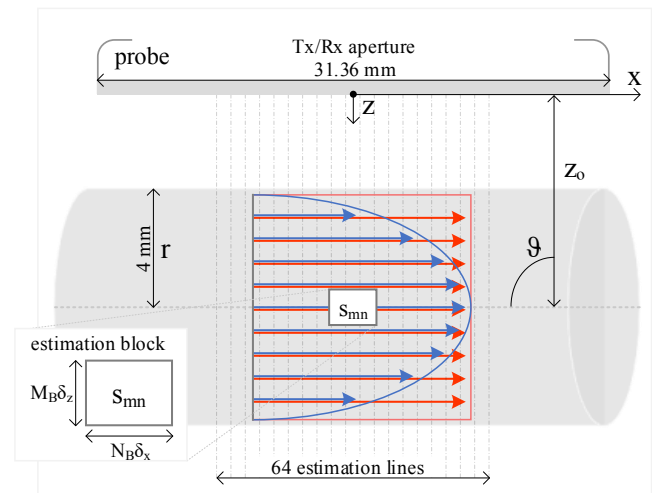


Fig. 1 Illustration of the reference system used for simulations. Flat (red) and parabolic (blue) flow profiles are highlighted. An HFR-VFI estimation block ( $S_{mn}$ ) is reported.

Specifically, the time between two consecutive frames is:

$$\tau = \frac{1}{PRF} \quad (1)$$

Couples of consecutive RF images are processed through the method proposed in [13]. The frames are divided into partially overlapped blocks of dimensions  $M_B \delta z$  (axial)  $\times$   $N_B \delta x$  (lateral), as sketched in Fig. 1, where  $\delta z$  and  $\delta x$  are the spatial distances between adjacent depths and lines, respectively. If the blood particles in a block move during the  $\tau$  interval, the block  $\tilde{s}_{mn}$  at time  $\tilde{t} = t + \tau$  can be assumed as a shifted version of the corresponding  $s_{mn}$  block at time  $t$ . Thus, the mean axial ( $\bar{v}_z$ ) and lateral ( $\bar{v}_x$ ) velocities within each block are estimated by computing the phase shifts ( $\Delta\Phi_{f_m n}$  and  $\Delta\Phi_{f_n m}$ ) in the frequency domain, as:

$$\bar{v}_z = \left[ \frac{1}{2n_f M_B} \sum_{n=1}^{N_B} \sum_{m=1}^{2n_f} \frac{M_B}{2\pi f_m} \Delta\Phi_{f_m n} \right] \frac{\delta z}{\tau} \quad (3)$$

$$\bar{v}_x = \left[ \frac{1}{2n_f^2} \sum_{n=1}^{n_f} \sum_{m=1}^{2n_f} \frac{N_B}{2\pi f_n} (\Delta\Phi_{f_m n} - \Delta\Phi_{f_n m}) \right] \frac{\delta x}{\tau} \quad (4)$$

with  $n_f$  the number of frequencies considered for the estimation, and  $m$  and  $n$  the indices in the axial and lateral directions, respectively.

### B. Simulation Set-up

Simulations were carried out by using Field II [16], [17] with main parameters set as listed in Table I. Specifically, PWs were transmitted at PRF=2500 Hz from an aperture of 128 elements. The transmission signal was a 5-cycle sinusoidal burst at central frequency  $f_0 = 6$  MHz tapered with a Hamming window.

Steady flow was simulated for both parabolic and flat profiles, both with a peak velocity of 15 cm/s. Simulations were conducted placing the axis of the tube at 5 different depths ( $z_0 = 2, 4, 6, 8$  and 10 cm) and 3 different angles ( $\theta = 90^\circ, 82.5^\circ$  and

TABLE I. SIMULATION SETUP

Probe Parameters	
Transducer	Linear Array
Number of Elements	192
Pitch [mm]	0.245
Central Frequency [MHz]	8
6dB Bandwidth	114%
Elevation Focus [mm]	18
System Parameters	
Speed of Sound (c) [m/s]	1540
Tx Central Frequency ( $f_0$ ) [MHz]	6
Rx Sampling Frequency ( $f_c$ ) [MHz]	50
Pulse Repetition Frequency (PRF) [Hz]	2500
Number of Tx/Rx Elements	128
Beamformed Lines	64
HFR-VFI Parameters	
Axial(z) block size ( $M_B \delta_z$ ) [mm]	1
Lateral(x) block size ( $N_B \delta_x$ ) [mm]	3.9
Number of frequencies ( $n_f$ )	5
Blood Flow Parameters	
Inner Radius [cm]	4
Beam-to-Flow Angle ( $\theta$ ) [°]	90, 82.5, 75
Barycentre Depth ( $z_0$ ) [cm]	2, 4, 6, 8, 10
Peak Velocity ( $v_p$ ) [cm/s]	15
Scatterers Density [ $1/\text{mm}^3$ ]	25

$75^\circ$ ). The density of scatterers was set to  $25/\text{mm}^3$ . For each set of scatterers, 500 consecutive PWs were transmitted, thus covering a 0.2 s time interval. The signals received from blood flowing inside a cylindrical tube (inner radius = 4 mm) were beamformed over 64 reception lines. RF images were reconstructed and processed as detailed in section II.A, with 1-mm-long and 3.9-mm-wide velocity estimation blocks.

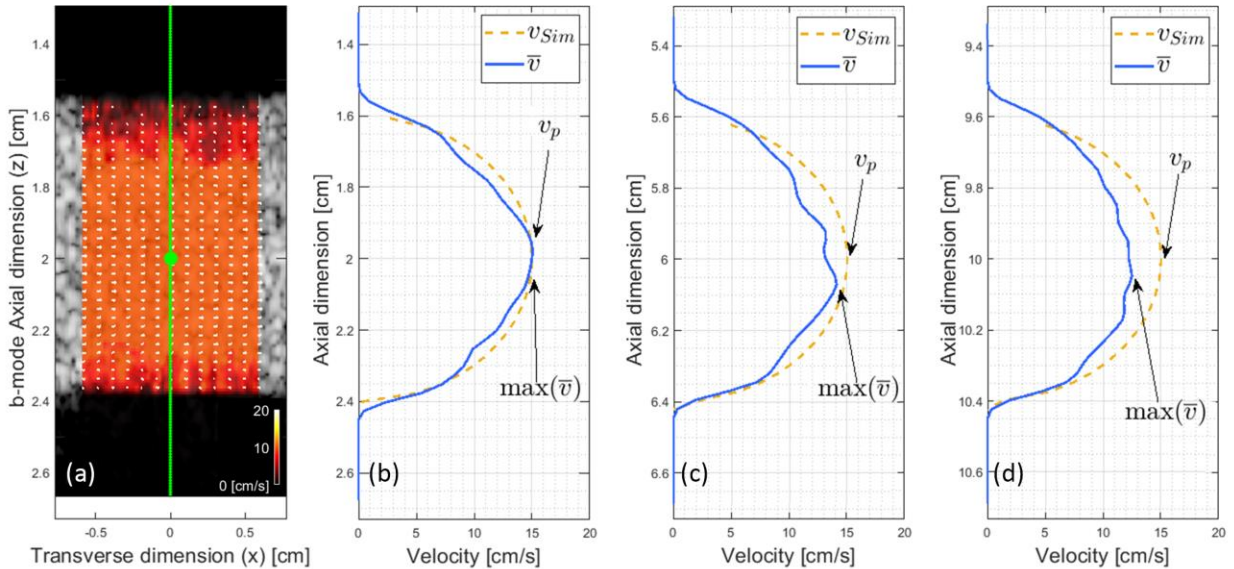


Fig. 2 (a) Typical vector map captured in parabolic flow simulation at 2 cm depth. The theoretical parabolic profile ( $v_{sim}$ ) is compared to the profiles ( $\bar{v}$ ) detected at depths of 2 (b), 6 (c) and 10 cm (d).

### C. Metrics

The HFR-VFI method accuracy was evaluated by computing the relative error on the velocity estimates as:

$$e = \frac{\max(\bar{v}) - v_p}{v_p} \% \quad (6)$$

where  $\bar{v}$  is the velocity profile estimated along the probe axis, averaged for all the frames, and  $v_p = 15 \text{ cm/s}$  is the ground-truth peak velocity. For example, the left panel of Fig.2 reports a typical frame detected at 2 cm depth, in which B-Mode is overlaid by the vector map and color-coded flow velocity. The green line represents the section where the velocity profile used for performance evaluation was selected. The three panels on the right show the ground-truth and the velocity profiles estimated at 2, 6 and 10 cm depth, respectively.

### III. RESULTS AND DISCUSSION

Fig. 3 shows the estimated peak velocity evaluated at 5 depths with 3 Doppler angles, for both the velocity profiles (parabolic and flat). The relative errors of peak velocity evaluated through eq. (6) are listed in Table II.

Parabolic flow results show that HFR-VFI is reasonably accurate at  $90^\circ$  ( $e < \pm 5\%$ ) for depths up to 6 cm. However, a considerable underestimation is noted at higher depths. In order to understand this behavior, we have evaluated in detail the pressure field obtained when a PW is transmitted. Fig. 4 shows the results of the pressure field simulations. The 5 panels (a)-(e) report the isolines (at -6dB steps) of the beamplots estimated on planes parallel to the probe surface. The transmitted beam keeps well its width on the lateral direction for all analyzed depths. In fact, the width is  $X_w=29.70 \text{ mm}$  at 2cm and reduces by only 0.6% only at 10 cm, where it reaches  $X_w=27.72 \text{ mm}$ . On the other hand, the beam shows a prominent progressive broadening, due to diffraction, on the y-direction. Here starting from  $Y_w=0.99 \text{ mm}$  at 2 cm it reaches  $Y_w=14.85 \text{ mm}$  at 10 cm, i.e. a widening of 1500%. It is worth highlighting that the -6dB width at 6 cm of depth ( $Y_w = 7.92 \text{ mm}$ ) is already comparable to the diameter of the simulated vessel (8 mm).

TABLE II. RELATIVE ERROR OF VELOCITY ESTIMATES

Depth	Parabolic Flow			Flat Flow		
	$\theta=90^\circ$	$\theta=82.5^\circ$	$\theta=75^\circ$	$\theta=90^\circ$	$\theta=82.5^\circ$	$\theta=75^\circ$
2 cm	2.1%	-2.9%	-8.7%	7.2%	6.9%	-0.4%
4 cm	5.0%	-11.5%	-4.0%	10.4%	3.4%	1.7%
6 cm	-2.7%	-22.7%	-26.1%	3.9%	-3.5%	-0.3%
8 cm	-13.8%	-31.3%	-22.6%	5.1%	-1.1%	-3.2%
10 cm	-14.7%	-35.5%	-30.4%	3.1%	-4.2%	-9.3%

Such a progressive azimuthal broadening may explain the velocity measurement results discussed above. In fact, such broadening corresponds to having huge “sample volumes” contributing to the instantaneous received echo signal. All particles present in the region excited by the pressure field are averaged in the frequency phase estimation. A parabolic flow features an azimuthal velocity gradient, so the estimate is decreased by the presence of components at lower velocity in the sample volume. This effect is even more accentuated at angles different from  $90^\circ$ , where the flow features a velocity gradient also in the lateral direction, as confirmed by the simulations (see Fig. 3).

The nominal extension of the estimation block size could, in principle, play a similar role, since the velocity contributions present in the area are averaged. However, this effect does not depend on depth (block size is virtually the same). Thus, at higher depths the underestimation seems to be mainly produced by the pressure field broadening.

This hypothesis is confirmed by the tests carried out for the flat flow, characterized by a constant velocity distribution over the entire vessel (red lines on Fig. 1). In this case there is no velocity gradient, the underestimation is reduced and the HFR-VFI is accurate both for different flow angles and depths of interests, showing an estimation error always lower than  $\pm 10\%$ .

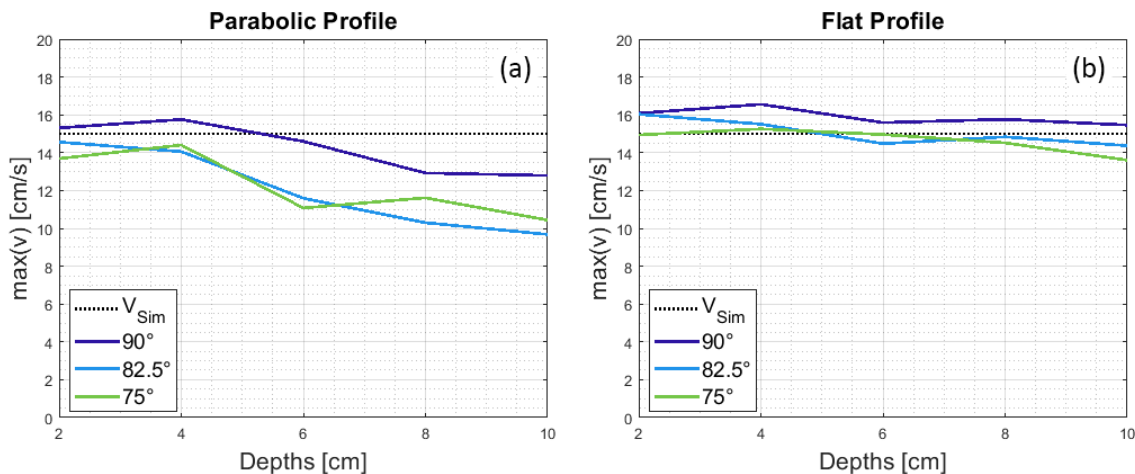


Fig. 3 Measured peak velocity module at different depth for parabolic flow (a) and flat flow (b)

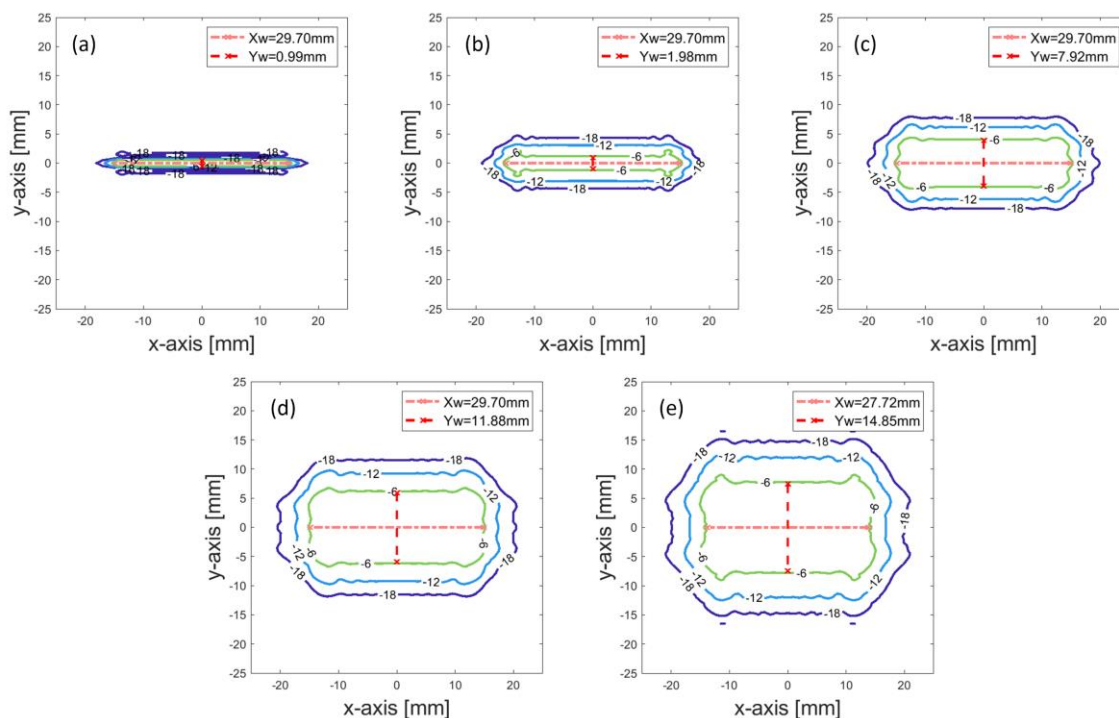


Fig. 4 Isolines of beamplots on planes parallel to the probe surface at 5 depths: (a) 20mm, (b) 40mm, (c) 60mm, (d) 80mm, (e) 100mm.

#### IV. CONCLUSION

The aim of this work was the evaluation of the performance attainable from PW-based vector flow imaging methods such as the HFR-VFI at great depths. The results show that the HFR-VFI method is suitable for the investigation of transverse flow in deep vessels, but the performance worsens for different flow orientations. However, to extend the application of any method based on plane wave TX to other flow orientations, it is necessary to control the beamwidth on the elevation plan, e.g. by a proper design of the acoustic lens or by using 1.5D or 2D arrays.

#### REFERENCES

[1] P. Tortoli, A. Dallai, E. Boni, L. Francalanci, and S. Ricci, "An Automatic Angle Tracking Procedure for Feasible Vector Doppler Blood Velocity Measurements," *Ultrasound Med. Biol.*, vol. 36, no. 3, pp. 488–496, Mar. 2010.  
 [2] S. Ricci, S. Diciotti, L. Francalanci, and P. Tortoli, "Accuracy and Reproducibility of a Novel Dual-Beam Vector Doppler Method," *Ultrasound Med. Biol.*, vol. 35, no. 5, pp. 829–838, May 2009.  
 [3] S. Ricci, A. Ramalli, L. Bassi, E. Boni, and P. Tortoli, "Real-Time Blood Velocity Vector Measurement Over a 2-D Region," *IEEE Trans. Ultrason. Ferroelectr. Freq. Control*, vol. 65, no. 2, pp. 201–209, Feb. 2018.  
 [4] F. Cikach, M. Y. Desai, E. E. Roselli, and V. Kalahasti, "Thoracic aortic aneurysm: How to counsel, when to refer," *Cleve. Clin. J. Med.*, vol. 85, no. 6, pp. 481–492, Jun. 2018.  
 [5] R. Steel, K. V. Ramnarine, F. Davidson, P. J. Fish, and P. R. Hoskins, "Angle-independent estimation of maximum velocity through stenoses using vector Doppler ultrasound," *Ultrasound Med. Biol.*, vol. 29, no. 4, pp. 575–584, Apr. 2003.  
 [6] R. Steel and P. J. Fish, "Error propagation bounds in dual and triple beam vector Doppler ultrasound," *IEEE Trans. Ultrason. Ferroelectr. Freq. Control*, vol. 49, no. 9, pp. 1222–1230, Sep. 2002.

[7] B. Dumire, K. W. Beach, K.-H. Labs, M. Plett, and D. E. Strandness Jr., "Cross-beam vector Doppler ultrasound for angle-independent velocity measurements," *Ultrasound Med. Biol.*, vol. 26, no. 8, pp. 1213–1235, Oct. 2000.  
 [8] J. A. Jensen and P. Munk, "A new method for estimation of velocity vectors," *IEEE Trans. Ultrason. Ferroelectr. Freq. Control*, vol. 45, no. 3, pp. 837–851, May 1998.  
 [9] M. J. Pihl and J. A. Jensen, "Measuring 3D velocity vectors using the Transverse Oscillation method," in *2012 IEEE International Ultrasonics Symposium*, 2012, pp. 1881–1885.  
 [10] R. Steel and P. J. Fish, "Velocity bias and fluctuation in the standard dual beam Doppler reconstruction algorithm," *IEEE Trans. Ultrason. Ferroelectr. Freq. Control*, vol. 49, no. 10, pp. 1375–1383, Oct. 2002.  
 [11] G. E. Trahey, J. W. Allison, and O. T. von Ramm, "Angle Independent Ultrasonic Detection of Blood Flow," *IEEE Trans. Biomed. Eng.*, vol. BME-34, no. 12, pp. 965–967, Dec. 1987.  
 [12] L. N. Bohs, B. J. Geiman, M. E. Anderson, S. C. Gebhart, and G. E. Trahey, "Speckle tracking for multi-dimensional flow estimation," *Ultrasonics*, vol. 38, no. 1–8, pp. 369–375, Mar. 2000.  
 [13] M. Lenge, A. Ramalli, E. Boni, H. Liebgott, C. Cachard, and P. Tortoli, "High-frame-rate 2-D vector blood flow imaging in the frequency domain," *IEEE Trans. Ultrason. Ferroelectr. Freq. Control*, vol. 61, no. 9, pp. 1504–1514, Sep. 2014.  
 [14] M. Lenge, A. Ramalli, P. Tortoli, C. Cachard, and H. Liebgott, "Plane-wave transverse oscillation for high-frame-rate 2-D vector flow imaging," *IEEE Trans. Ultrason. Ferroelectr. Freq. Control*, vol. 62, no. 12, pp. 2126–2137, Dec. 2015.  
 [15] S. Rossi, M. Lenge, A. Dallai, A. Ramalli, and E. Boni, "Toward the Real Time Implementation of the 2-D Frequency-Domain Vector Doppler Method," 2019, pp. 129–135.  
 [16] J. A. Jensen and N. B. Svendsen, "Calculation of pressure fields from arbitrarily shaped, apodized, and excited ultrasound transducers," *IEEE Trans. Ultrason. Ferroelectr. Freq. Control*, vol. 39, no. 2, pp. 262–267, Mar. 1992.  
 [17] J. A. Jensen, "FIELD: A Program for Simulating Ultrasound Systems," *Med. Biol. Eng. Comput.*, vol. 34, no. Supplement 1, Part 1, pp. 351–353, 1996.